



Supported by



Accepted Article

Title: NNN Pincer-functionalized porous organic polymer supported Ru(III) as a heterogeneous catalyst for levulinic acid hydrogenation to γ -valerolactone

Authors: Kwangho Park, Sudakar Padmanaban, Seong-Hoon Kim, Kwang-Deog Jung, and Sungho Yoon

This manuscript has been accepted after peer review and appears as an Accepted Article online prior to editing, proofing, and formal publication of the final Version of Record (VoR). This work is currently citable by using the Digital Object Identifier (DOI) given below. The VoR will be published online in Early View as soon as possible and may be different to this Accepted Article as a result of editing. Readers should obtain the VoR from the journal website shown below when it is published to ensure accuracy of information. The authors are responsible for the content of this Accepted Article.

To be cited as: *ChemCatChem* 10.1002/cctc.202001376

Link to VoR: <https://doi.org/10.1002/cctc.202001376>

NNN Pincer-functionalized porous organic polymer supported Ru(III) as a heterogeneous catalyst for levulinic acid hydrogenation to γ -valerolactone

Kwangho Park,^[a] Sudakar Padmanaban,^[b] Seong-Hoon Kim,^[c] Kwang-Deog Jung,^[a] and Sungho Yoon*,^[c]

[a] Dr. K. Park and Dr. K. D. Jung
Clean Energy Research Centre
Korea Institute of Science and Technology
P.O. Box 131, Cheongryang, Seoul (Republic of Korea)

[b] Dr. S. Padmanaban
Department of Chemistry
Seoul National University
1 Gwanak-ro, Gwanak-gu, Seoul (Republic of Korea)

[c] Dr. S. H. Kim and Dr. Prof. S. Yoon*
Department of Chemistry
Chung Ang University
84 Heukseok-ro, Dongjak-gu, Seoul, Republic of Korea
E-mail: sunghoyoon@cau.ac.kr
Supporting information for this article is given via a link at the end of the document.

Abstract: A novel porous organic polymer that incorporates NNN pincer type of ligand, i.e., 2,6-Bis(pyrazol-3-yl)pyridine, (3-bpp-POP) is prepared via solvent-knitting method. Through the characterizations, 3-bpp-POP is demonstrated to possess abundant porous structure, high surface area, and excellent thermal durability. A ruthenium molecular catalyst immobilized on the 3-bpp-POP support exhibits substantial catalytic performance for the hydrogenation of LA to GVL with an initial turnover frequency (TOF) of 1680 h⁻¹ and a maximum turnover number (TON) of 14762 over 24 h for LA conversion with selectivities of 91.1 % for GVL and 8.9 % for HPA. The catalyst demonstrated excellent durability during successive recycles without leaching Ru³⁺, which ascribe to the strong binding of pincer ligand to metal centers.

Introduction

Porous organic polymers (POPs) are of great interest as catalytic supports for various catalytic applications because they exhibit micro- or mesoporosity, high surface area, and high robustness under harsh catalytic conditions.^[1-5] In particular, POPs show promise as novel catalyst supports because their physicochemical properties can be manipulated at the molecular level through the rational design of monomers and linking strategies. Recently, POP-supported transition-metal-based catalysts have attracted considerable attention, because they combine the properties of homogeneous and heterogeneous catalyst systems.^[6-9] The development of new and diverse POP structures remains a challenge in the field of catalytic research.

Hyper-crosslinked porous polymers (HCPs) are a subclass of POPs prepared by solvent-knitting via a Lewis-acid-promoted Friedel-Crafts reaction; they have attracted significant attention in the field of catalysis.^[10-13] Due to their intrinsic porosity and stability, which is derived from stable C-C cross-coupling of the aromatic groups on the building blocks, HCPs have been explored as catalysts and catalyst supports in various catalytic systems. In addition, the inexpensive, user-friendly synthetic process is desirable for the scaled-up preparations required for industrial operation. In particular, HCP-based catalysts

incorporating preserved molecular ligand sites or structures analogous to homogeneous metal complex catalysts have demonstrated excellent catalytic activity and stability for several catalytic conversions.^[14]

The hydrogenation of biomass-derived levulinic acid (LA) to γ -valerolactone (GVL) shows promise in sustainable and eco-friendly chemical production.^[15-19] Multiple studies have used homogeneous and heterogeneous catalysts to produce an affordable supply of GVL from bio-derived LA.^[20-26] In heterogeneous-catalyzed LA hydrogenation reactions, commercial Ru/C catalyst exhibited high catalytic efficiency and deactivated rapidly due to leaching and aggregation. Numerous devotion to improving stabilization of Ru NPs on catalyst supports have been implemented, resulting from the combination of Ru NPs and metal oxide catalyst supports, such as Al₂O₃, TiO₂, ZrO₂, and heteroatom-doped carbons.^[27-43] However, it is still advisable to investigate further the synergetic combination of Ru NPs and catalyst supports to escape from deactivation over subsequent cycles or in continuous flow production.

Therefore, the fabrication of catalyst supports with well-defined functional metal binding sites is highly desired,^[44-45] and recently POP supported metal catalysts have been reported, featuring effectiveness and high stability. Wang et al. reported that Ru NPs could be immobilized on ionic mesoporous polymer supports via an efficient synergetic interaction between Ru NPs and the anions and amide groups on the support surface; the resulting catalysts exhibited improved stability as well as catalytic activity.^[46] Recently, Shen et al. prepared robust, porous Ir-, Ru-, and Pd-based organometallic polymers via a direct knitting approach, using the Friedel-Crafts reaction as a crosslinking strategy.^[47] The porous organometallic catalyst with incorporated N-heterocyclic carbene metal complexes exhibited excellent activity and selectivity with high robustness for the hydrogenation of LA to GVL. Despite the promising results of POP-supported transition metal catalysts, a small number of studies have been reported for LA hydrogenation. The development of an immobilized molecular catalyst system with a

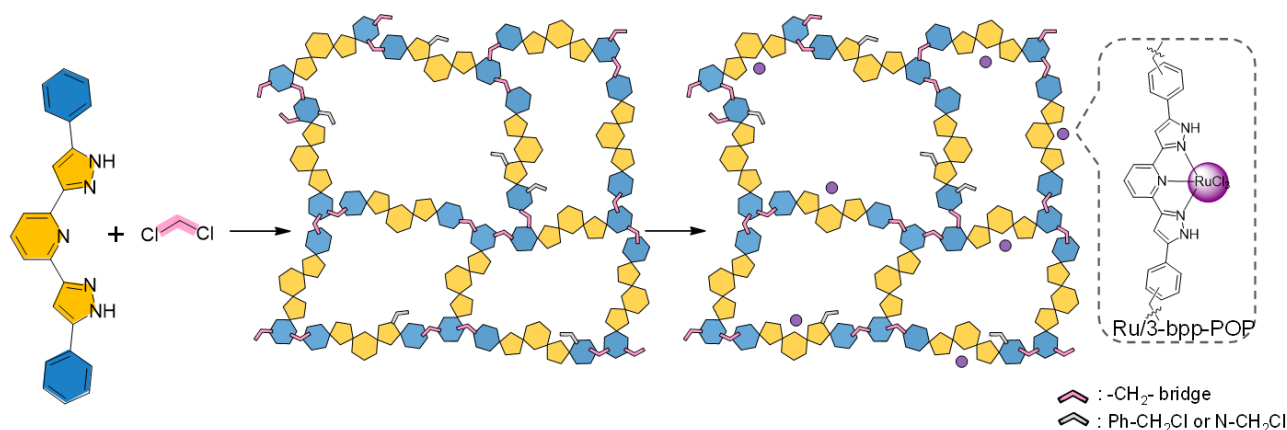


Figure 1. Structural representation of Ru/3-bpp-POP synthesis

novel POP remains a significant challenge to achieve commercial feasibility for the biomass-derived economy.

2,6-Bis(pyrazol-3-yl)pyridine is a well-known pincer-type ligand that provides adjacent NNN-coordination to metal units. Strong tridentate coordination with the metal center produces highly stable pincer complexes. The electronic and steric properties of 3-bpp ligands are tunable, and multiple transition metal-based 3-bpp complexes have been reported for diverse catalytic applications.^[48-54] Ru complexes of 3-bpp ligand derivatives have demonstrated high catalytic efficiencies for ketone-to-alcohol transfer hydrogenation, a key step in the hydrogenation of LA to GVL.^[55-57] A heterogeneous Ru molecular catalyst with 3-bpp-based POPs, combining the function of the Ru 3-bpp catalyst system with the advantage of a solid support, would be of interest for both scientific and industrial applications.

Here, we present a 2,6-bis(5-phenyl-1H-pyrazol-3-yl)pyridine-based porous organic polymer (3-bpp-POP) as a novel support to immobilize a Ru-based catalyst (**Figure 1**). The Ru/3-bpp-POP catalyst exhibits efficient catalytic hydrogenation of LA to GVL compared to its homogeneous counterpart, with an initial turnover frequency (TOF) of 1680 h⁻¹ and a maximum turnover number (TON) of 14762 over 24 h for LA conversion with selectivities of 91.1 % for GVL and 8.9 % for HPA. When recovered by filtration, the catalyst remains immobilized and retains its catalytic efficiency over successive batch reactions. The catalyst exhibits no Ru metal leaching or support degradation during catalysis, due to strong binding between the Ru-based catalytic sites and the pincer-type bpp ligand moiety on the support

Results and Discussion

The aryl substituent building block for the knitting method, i.e. 2,6-bis(5-phenyl-1H-pyrazol-3-yl)pyridine (3-bpp), was synthesized according to a previously reported procedure.^[58] The 3-bpp-POP was prepared by crosslinking aryl substituents on the bpp monomer using dichloromethane as a solvent and linking agent, promoted by an AlCl₃-catalyzed Friedel-Crafts reaction. The afforded polymer was insoluble in common organic solvents such as acetone, methanol, and tetrahydrofuran under Soxhlet extraction and washing step, which is due to the cross-linked structure. Analysis by scanning electron microscopy

(SEM) indicated that the 3-bpp-POP support possesses irregularly shaped particles of size 10–30 μm (Figure 2a). Electron-dispersive X-ray spectroscopy (EDX) confirmed that the C and N atoms from the bpp units are distributed homogeneously throughout the catalyst support. Additionally, AlCl₃ was absent from the structure, indicating that it had been effectively removed after the Friedel-Crafts reaction (Figure S1 and Table S1).

The porosity of 3-bpp-POP was assessed by N₂ adsorption-desorption isotherm analysis at 77 K. N₂ sorption of the support (Figure 2b) showed stiff adsorption capacity of N₂ at p/p₀ < 0.05 with a typical type-IV isotherm shape, which indicate abundant presence of micropores and mesopores in the polymer support.^[59] The Brunauer-Emmett-Teller (BET) surface area of the 3-bpp-POP support is 565.8 m² g⁻¹, featuring a mean pore diameter of 2.1 nm and total pore volume of 0.29 cm³ g⁻¹. We expect this high porosity and surface area to enable the effective dispersion of metal complexes, as well as mass transfer of the reactants to catalytic active sites.

The thermal stability of the 3-bpp-POP was evaluated by thermogravimetric analysis (TGA). The support was highly durable at temperatures up to 400 °C, exhibiting only ~3% weight loss, except for moisture evaporation from the pore structures (Figure 2c, blue line). In addition, the initial decomposition temperature increased from 310 °C for the monomer (Figure 2c, gray line) to 370 °C for the 3-bpp-POP, indicating improved thermal durability of the POP structure, resulting from crosslinked networks in the polymer. Elemental analysis was performed to determine the precise atomic composition of the catalyst support. For the evaluation of the elemental composition, the C/N ratio was chosen because captured residual moisture and Cl in the 3-bpp-POP could not be included in the result with this analysis method. The C/N ratio of the 3-bpp-POP was 4.89, compared to 3.85 for the bpp monomer (Table 1). The increased carbon content is attributed to the addition of -CH₂- bridges during polymerization via C-C crosslinking.

Fourier-transform infrared (FT-IR) spectroscopy was conducted to characterize the chemical structure of the 3-bpp-POP. The IR spectrum of the catalyst support (Figure 2d, blue line) contains vibrational absorption bands at 3400, 3200 (-NH), 3000 (-CH₂-), 1630 (-C=N), 1596, 1565, 1445, 1282, 1155, 1052, 991, 959, 900, and 804 cm⁻¹. Intact functional groups, such as N-H, C-H, C-N, and C=N, originating from the phenyl, pyridine,

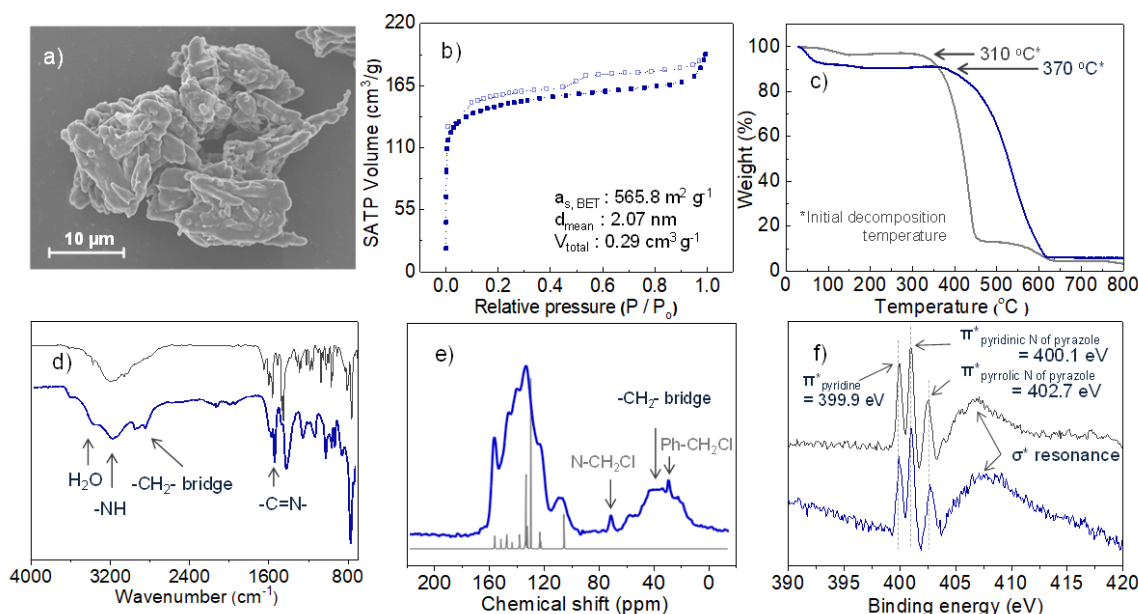


Figure 2. Characterization of 3-bpp-POP. a) SEM image; b) N₂ sorption isotherms analysis; c) TGA; d) FT-IR spectra; e) ¹³C NMR spectra; and f) NEXAFS. (blue line for 3-bpp-POP and gray line for 3-bpp monomer)

Table 1. Elemental analysis of 3-bpp monomer and 3-bpp-POP.

Sample	C	N	H	C/N	C/N
bpp monomer	72.84	18.94	5.1	3.85	3.94
bpp-POP	62.11	12.69	5.64	4.89	bpp + n(-CH ₂ -)

and pyrazole moieties of bpp are present. In particular, the vibration peaks in the 3-bpp-POP spectrum are similar to those found in the regional absorption band of the bpp moiety, confirming that the original structure of the bpp moiety is well preserved in the polymer (Figure 2d, gray line). Magic-angle-spinning solid-state nuclear magnetic resonance spectroscopy (MAS ssNMR) was performed to gain more detailed chemical structural information of 3-bpp-POP. The spectra of ¹H MAS ssNMR showed rather broad lumps of signals, which is attributed to the strong dipolar couplings of protons with little-motional averaging in solid structure (Figure S6).^[60, 61] Deconvolution of the spectra support the presence of aliphatic groups from -CH₂- bridge at around 3.6-4.5 ppm, aromatic groups from 3-bpp moiety at around 6.5-8.0 ppm, and pyrazolyl NH groups at around 12.5-13.5 ppm. Upon the ¹³C cross-polarization MAS ssNMR (¹³C CPMAS ssNMR), signals were observed at 152.4, 141.7, 129.0, 119.1, and 104.6 ppm which are assigned to the distinctive carbon signals of functional groups on phenyl, pyridine, and pyrazole (Figure 2e, blue line). The results are similar to those found in the ¹³C NMR spectrum of the 3-bpp monomer, confirming that the 3-bpp moiety is intact (Figure 2e, gray line). Importantly, a new broad peak at 10–60 ppm is observed for bpp-POP; this is the typical signal region for alkyl groups and confirms the presence of abundant -CH₂-bridges in the polymer structure resulting from C-C crosslinking.^[62, 63] Meanwhile, clear resonance peaks with low intensity at 28 and 70 ppm were observed, which indicate partial side reactions on 3-bpp-POP support such as un-crosslinking (Ph-CH₂Cl) and N-alkylation (N-CH₂Cl) on pyrazolyl N sites.

X-ray photoelectron spectroscopy (XPS) was conducted to understand the chemical state of C and N components of 3-bpp-POP. (Figure S8) Through the deconvolution of binding energy peaks, it was confirmed that 3-bpp-POP showed C-C at 284.6 eV and C-N at 286.0 eV for C 1s. (Figure S12a) Also the POP support exhibited three deconvoluted peaks for N 1s; pyridinic N at 398.6 eV and 399.3 eV, assigned to pyridine and pyrazole, respectively, and Pyrrolic N at 400.6 eV (Figure S12b). Meanwhile, the Cl 2p XPS peak was shown in very low intensity and deconvoluted into one set of double peaks at 199.8 eV for Cl 2p_{3/2} of -CH₂-Cl and at 201.5 eV for Cl 2p_{1/2} of -CH₂-Cl, which indicates the partial side reactions of Friedel-Crafts reaction (Figure S12c).

Synchrotron-based near-edge X-ray absorption fine structure (NEXAFS) was performed to clarify chemical bonding in the polymer support (Figure 2f, blue line). The carbon K-edge spectrum of the 3-bpp-POP revealed four resonances: at 284.8 eV, assigned to π*_{C=C} at for aromatic rings; at 285.5 and 288.1 eV, assigned to π*_{C=C} and π*_{C-N-C}, respectively, in pyridine and pyrazole; and at 292.0–300 eV, assigned to σ*_{C-C} (Figure S7). In the nitrogen K-edge spectrum, the 3-bpp-POP exhibited three distinctive π* resonances, occurring at 399.9 eV for pyridine, 400.1 eV for pyridinic N, and 402.7 eV for the pyrrolic N in pyrazole, as well as a broad σ* resonance over the range 403–415 eV.^[64, 65] These results match those obtained with the 3-bpp-monomer (Figure 2f, gray line), providing crucial evidence for the presence of intact 3-bpp moieties on the surface of the polymer support.

Successful incorporation of Ru catalysts on the 3-bpp-POP support was achieved via post-synthetic metalation; a methanolic solution of RuCl₃ xH₂O was added to an equal volume of support-dispersed methanol solution in inert atmosphere. The accurate Ru content in the catalyst was determined to be 3.02 wt% via inductively coupled plasma optical emission spectroscopy (ICP-OES). Given that the result of elemental analysis together, the incorporation efficiency of RuCl₃ on the 3-bpp-POP support was determined as around

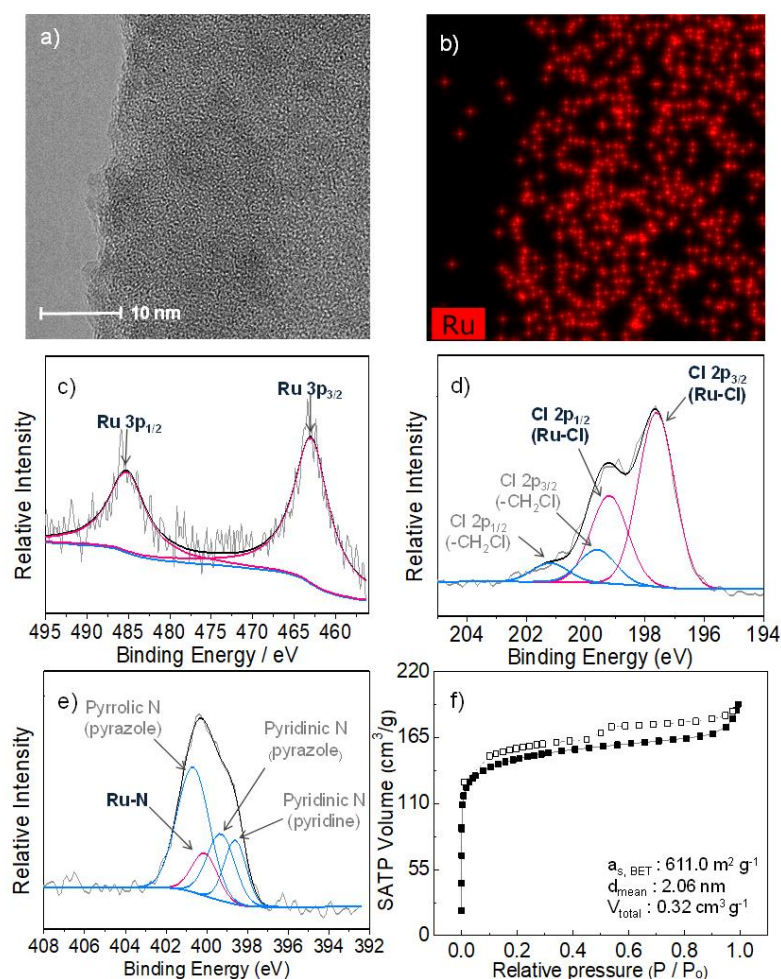


Figure 3. Characterizations of Ru/3-bpp-POP. a) HR-TEM image; b) EDX mapping image for Ru; c) deconvoluted Ru 3p; d) Cl 2p; e) N 1s XPS spectra; f) N₂ sorption isotherms analysis

16 %, which indicates every six 3-bpp moiety on the POP support contains one RuCl₃ unit. High-resolution transmission electron microscopy (HR-TEM) combined with EDX verified the absence of Ru nanoparticles, while RuCl₃ species were homogeneously distributed throughout the catalyst support (Figure 3a,b). X-ray photoelectron spectroscopy (XPS) was performed to characterize the electronic state and coordination environment of the molecular Ru catalyst on the 3-bpp-POP support. The binding energies of Ru 3d_{3/2} and Ru 3p_{3/2} for the Ru/3-bpp-POP catalyst were 282.0 eV and 463.0 eV, respectively, indicating that the Ru species maintained its original oxidation state of Ru³⁺ in the catalyst (Figure 3c).^[66] In addition, the Cl 2p XPS profile of Ru/3-bpp-POP is deconvoluted into two sets of double peaks: Cl 2p_{3/2} of Ru-Cl at 197.6 eV in RuCl₃ and Cl 2p_{3/2} of -CH₂-Cl at 199.7 eV in the 3-bpp-POP support (Figure 3d and Figure S9). The N 1s XPS profile of Ru/3-bpp-POP was deconvoluted into four peaks at 398.7, 399.3, 400.0, and 401.0 eV (Figure 3e). In contrast, only three sets appear in the spectrum of the 3-bpp-POP support, which are assigned to the pyridinic N and pyrrolic N on pyrazole. The emergence of a fourth peak at 400.0 eV in the Ru/3-bpp-POP spectrum is attributed to coordination of the Ru species to the pyridinic N, also supported by previous reports. Thus, it is confirmed that the RuCl₃ species is stabilized on the catalyst by N-based binding sites on the 3-bpp ligand moiety. In addition,

the catalyst maintained its porous structure after metalation (Figure 3f); BET surface area is 611.0 m² g⁻¹, featuring mean pore diameter of 2.04 nm and total pore volume of 0.32 cm³ g⁻¹. The slight increase of surface area for Ru/3-bpp-POP compared to that of catalyst support may be ascribed to the swelling effect during the metalation process.

The catalytic activity of Ru/3-bpp-POP for LA hydrogenation was assessed in a batch reactor; various reaction conditions such as solvents, temperature, pressure, and reaction time, were evaluated and outcomes of the batch reactions are listed in Table 2. Efficient LA hydrogenation has been reported under protic solvents such as water and methanol, which help to facilitate the hydride transfer in hydrogen cleavage step by accepting and donating protons.^[26, 67-70] Therefore, in this study, water and methanol was chosen for the catalytic activity screening of LA hydrogenation. However, the Ru/3-bpp-POP catalyst exhibited very low activity under aqueous conditions (Table 2, entry 1), because it floated on the solvent surface or stuck to the walls of the batch reactor during operation; we attribute this to the low density of the catalyst. Further, the catalyst demonstrated low selectivity for GVL in methanol (Table 2, entry 2); thus, a mixture of water and methanol was selected as the solvent for typical catalytic reactions (Table 2, entry 3). As such, hydrogenation over Ru/3-bpp-POP was initially performed with water and methanol as the solvent.

Table 2. Batch reactions^[a]

Entry	Solvent	T	P ^[b]	LA/Ru	Time	Conversion ^[c]	GVL yield ^[c]	HPA yield ^[c]	TON (TON _{GVL}) ^[d]
		[°C]	[bar]	S/C					
1	H ₂ O	120	50	1500	2	-	-	-	-
2	MeOH	120	50	1500	2	31.2	63.8	36.2	468 (298)
3	MeOH+H ₂ O	120	50	1500	2	23.0	83.5	16.5	345 (288)
4	MeOH+H ₂ O	100	50	1500	2	2.8	77.8	22.2	41 (32)
5	MeOH+H ₂ O	140	50	1500	2	68.6	87.1	12.9	1029 (897)
6	MeOH+H ₂ O	160	50	1500	2	98.4	88.7	11.3	1476 (1310)
7	MeOH+H ₂ O	160	10	1500	2	26.3	92.3	7.7	394 (364)
8	MeOH+H ₂ O	160	30	1500	2	86.6	86.8	13.2	1300 (1128)
9 ^[e]	MeOH+H ₂ O	160	50	15000	0.5	5.6	92.3	7.7	840 (776)
10 ^[e]	MeOH+H ₂ O	160	50	15000	2	16.9	91.9	8.1	2535 (2330)
11 ^[e]	MeOH+H ₂ O	160	50	15000	6	38.6	92.0	8.0	5792 (5328)
12 ^[e]	MeOH+H ₂ O	160	50	15000	15	89.6	92.1	7.9	13443 (12381)
13 ^[e]	MeOH+H ₂ O	160	50	15000	24	98.4	91.1	8.9	14762 (13442)

[a] Reaction conditions (unless otherwise stated): 20 mg of Ru/3-bpp-POP in 20 ml solvent, solvent combination of MeOH and H₂O at 1:1 (vol/vol) was used, and at 250 rpm of stirring rate [b] Pressure at ambient temperature [c] Values were based on ¹H NMR spectroscopy with maleic acid as internal standard, [d] TON = mol_{GVL+HPA}/mol_{Ru}, or TON_{GVL}=mol_{GVL}/mol_{Ru}, [e] 60ml of solvent with combination of MeOH and H₂O at 1:1 (vol/vol)

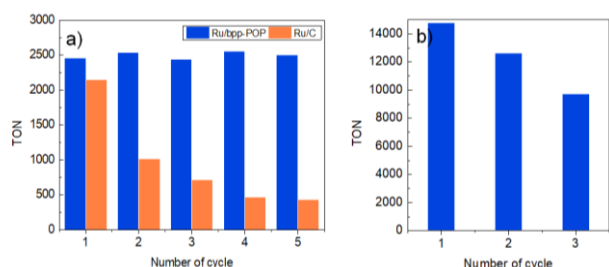


Figure 4. Recyclability tests of Ru/3-bpp-POP and commercial Ru/C catalyst

The effect of temperature on the catalytic performance of Ru/3-bpp-POP was evaluated at 50 bar. The catalyst showed only 2.8% conversion of LA at 100 °C and 50 bar (Table 2, entry 4). However, the catalytic performance proportionally increased at elevated temperatures, affording 98.4% conversion of LA at 160 °C with selectivities of 88.7% for GVL and 11.3% for HPA (Table 2, entry 6). While carrying out time-dependent studies, an

initial TOF of 1680 h⁻¹ and a maximum turnover number (TON) of 14762 over 24 h for LA conversion with selectivities of 91.1 % for GVL and 8.9 % for HPA were obtained. (Table 2, entry 9-13 and Figure S16) Interestingly, these results are similar to those reported previously for a homogeneous Ru catalyst with N-based ligands, suggesting that the immobilized Ru/3-bpp-POP catalytic site functions similarly to its homogenous counterparts.^[71] However, the catalytic activity of Ru/3-bpp-POP decreased to 86.6% at 30 bar and 26.3% at 10 bar; therefore, the total reaction pressure was maintained at 50 bar. (Table 2, entry 7 and 8)

The recyclability of Ru/3-bpp-POP was studied in subsequent batch reactions in optimized condition at 160 °C and 50 bar for 2h (Table S3). Firstly, a hot-filtration experiment was performed; no catalytic function was observed in the filtered solution over a prolonged reaction time, confirming stable immobilization of the catalyst (Figure S16, red line). The spent catalyst was recycled by simple filtration and subsequently charged into the batch reactor. The catalyst retained its activity after five cycles (Figure 4a, blue column). To check for the presence of leached Ru in the reaction feed, ICP-OES was

performed; negligible loss of Ru content from the catalyst was detected. The additional recycle tests were conducted using a commercial Ru/C catalyst with the same reaction conditions for comparison; a significant deactivation was observed during successive runs (Figure 4a, orange column). The improved stability of Ru/3-bpp-POP verifies stable coordination between the bpp ligands and the Ru species at the active sites.

The recycled catalyst was collected after stability tests and was further characterized by TEM-EDX, N₂ sorption isotherm analysis, FT-IR, and XPS to assess any chemical or structural changes. HAADF-STEM and EDX analyses revealed that the spent catalyst was covered with small particles of Fe metal throughout the catalyst surface, which may be ascribed to contamination from the reactor (Figure S5). Therefore, it is unsuccessful to find out the generation of Ru nanoparticles. However, it was confirmed that the Ru components remained homogeneously dispersed on the 3-bpp support by EDX (Figure 5a). To further prove whether Ru nanoparticles are generated during hydrogenation, poisoning experiments were conducted with PMe₃ as poisoning agents (Table S4). It is reported that the treatment of poisoning agents in the substoichiometric amount to the nanoparticle-based catalytic reaction could stop the catalytic conversion.^[72] On the contrary, the result of the poisoning study with fresh and spent Ru/3-bpp-POP catalysts showed that both catalysts retained its original catalytic activity, demonstrating that the active catalysts are immobilized molecular Ru species on 3-bpp-POP support. The oxidation state of Ru was also assessed using XPS analysis. The Ru 3d_{5/2} and Ru 3p_{3/2} binding energies of the Ru species on the spent catalyst were 281.6 eV and 462.7 eV, consistent with retained Ru³⁺ oxidation state; the slight decrease in binding energy compared to that of the fresh catalyst may be attributed to the substituted hydride, which has a greater electron donation effect than the chloride ligand (Figure 5b). The Cl 2p peak was disappeared in the recovered catalyst which supports ligand substitution.

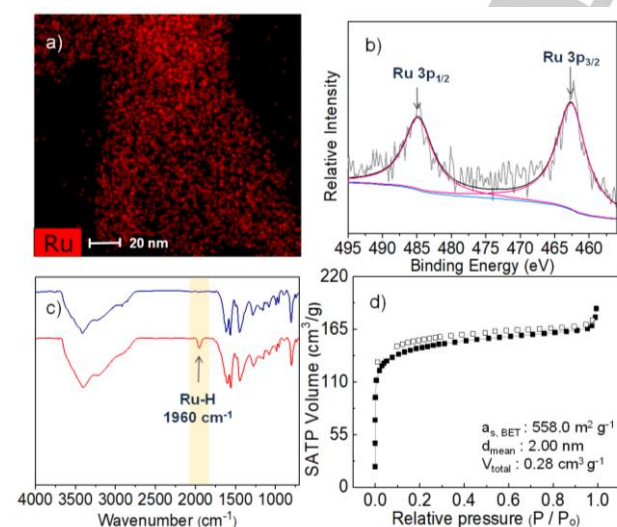


Figure 5. Characterization of the spent Ru/3-bpp-POP. a) EDX mapping image; b) deconvoluted Ru 3p XPS spectrum; c) FT-IR (blue line for the fresh catalyst and red line for the spent catalyst); d) N₂ sorption isotherms analysis

Electron paramagnetic resonance (EPR) was also performed to verify the change of Ru oxidation state in the spent catalyst (Figure S25). The EPR spectrum of Ru/bpp-POP showed signals at $g_1=2.265$, $g_2=2.085$, and $g_4=1.902$ which

suggests the presence of Ru 3+ species; Ru 2+ is silent in EPR.^[73-75] In addition, the IR spectrum of the spent catalyst was almost identical to that of the fresh catalyst, confirming high robustness of the catalyst support. Importantly, the freshly emerged peak at 1960 cm⁻¹ for the spent catalyst indicates the generation of a Ru-hydride species during hydrogenation (Figure 5c), which was stable under ambient conditions also.^[76, 77] The porosity of the spent catalyst was also evaluated with N₂ adsorption-desorption analysis at 77 K. The porosity of the catalyst was very similar to that of the fresh catalyst, indicating that no structural degradation or decomposition of the support occurred during hydrogenation (Figure 5d). However, in a 24h-term catalyst recycling test, a decrease in catalytic activity was observed, reaching a TON of 9718 in the third cycle (Figure 4b and Table S3).

Conclusion

In summary, a novel porous organic polymer that incorporates NNN pincer type ligand was prepared via solvent-knitting method. The 3-bpp-POP demonstrated to possess excellent thermal durability, abundant micro- and mesopore structure, and high surface area. A supported-ruthenium molecular catalyst on the 3-bpp-POP with the privileged properties as catalyst support exhibited substantial catalytic performance for the hydrogenation of LA to GVL with an initial turnover frequency (TOF) of 1680 h⁻¹ and a maximum turnover number (TON) of 14762 over 24 h for LA conversion with selectivities of 91.1 % for GVL and 8.9 % for HPA. The catalyst was also demonstrated excellently durable during successive recycles without leaching Ru³⁺, which ascribed to the strong binding of pincer ligand to metal centers. This study may provide insights in search of the strategies for incorporating the pincer-type ligands or complexes on porous organic polymers that successfully function as heterogeneous catalysts. We have extended this synthetic approach to additional heteroatom-containing POP supports, such as phosphine and sulfur, as part of our ongoing research.

Experimental Section

Materials and instrumentation

All chemicals were purchased from commercial companies and used without purification. Acetophenone (>99%) and diethyl 2,6-pyridinedicarboxylate (>98%) were purchased from T.C.I. Chemicals. Ruthenium chloride hydrate (RuCl₃ · xH₂O), aluminum chloride (AlCl₃) (>99%), sodium hydride 60 % dispersion in mineral oil, lithium chloride, hydrazine monohydrate, anhydrous methylene chloride, anhydrous tetrahydrofuran, and anhydrous methanol were purchased from Sigma Aldrich. Hydrochloric acid solution was purchased from Daejung chemical & metals. H₂ gas cylinder was obtained from Sinyang Gas Industries. 2,6-bis(5-phenyl pyrazolyl)pyridine was synthesized according to a previous report with modifications.⁵⁷

Fourier transform infrared (FT-IR) analysis was conducted on a Nicolet iS 10 with an MCT detector (Thermo Fisher Scientific) using KBr pellet technique. Scanning electron microscopy (SEM) and Electron-dispersive X-ray spectroscopy (EDX) measurements were carried out on a JEOL LTD (Japan) JEM-7610F operated at an accelerating voltage of 20.0 kV. N₂ adsorption-desorption measurements were performed at 77 K using a

BELSORP mini II (Japan). The samples were dried for 1 day at 150 °C before the analysis. Elemental analysis (EA) was conducted with an elemental analyzer (Vario Micro Cube, Germany). Thermogravimetric analysis (TGA) and differential thermal analysis (DTA) were conducted on a Q600 analyzer (TA Instrument, US). The experiments were performed at a heating rate of 10 °C per minute up to 700 °C under a nitrogen atmosphere. The ruthenium content was analyzed by inductively coupled plasma optical emission spectrometry (ICP-OES) (ICP-OES 720, Agilent) using a microwave-assisted acid digestion system. X-ray photoelectron spectroscopy (XPS) analysis was carried out on an ESCA 2000 (VG Microtech) at a pressure of $\sim 3 \times 10^{-9}$ mbar using Al K α as the excitation source ($h\nu = 1486.6$ eV) with a concentric hemispherical analyzer. High-angle annular dark-field imaging transmission electron microscopy (HAADF-TEM) analyses were carried out on a JEOL JEM-2100F HRTEM operated at 200 kV. The samples were prepared by dispersing in ethanol and dropped on a carbon film grid and analyzed after drying under vacuum at 60 °C overnight. X-ray absorption spectroscopy measurements were performed at 10D XAS KIST beamline in Pohang Light Source (PLS-II, 3.0 GeV, South Korea). ^{13}C and ^1H NMR spectra were analyzed on a Bruker Ascend 400 MHz. ^{13}C CPMAS solid state NMR data were attained at ambient temperature on 400 MHz Solid state NMR spectrometer (AVANCE III HD, Bruker, Germany) at KBSI Western Seoul center with an external magnetic field of 9.4 T. The operating frequency was 100.66 MHz for ^{13}C and the spectra were referenced relative to TMS. The samples were contained in HX CPMAS probe, with 4 mm o.d. Zirconia rotor. EPR measurements were carried out at KBSI Western Seoul Center, Korea. CW X-band (9.64 GHz) EPR spectra were collected on a Bruker EMX plus 6/1 spectrometer equipped with an Oxford Instrument ESR 900 liquid He cryostat using an Oxford ITC 503 temperature controller. All spectra were collected with the following experimental parameters: microwave power, 1 mW; modulation amplitude, 10 G; 3 scans; temperature, 10 K.

Synthesis of 3,3'-(pyridine-2,6-diyl)bis(1-phenylpropane-1,3-dione)

Acetophenone (5.75 ml, 49.3 mmol) was added to a suspension of NaH (dispersed in mineral oil) (2.37 g, 59.3 mmol) in 100 ml of THF. The mixture was stirred for 1 h under nitrogen atmosphere and then heated to reflux. Diethyl pyridine-2,6-dicarboxylate (5.00 g, 22.4 mmol) in 150 ml of THF was added to the boiling mixture for 30 min with additional funnel and the mixture was maintained at reflux for an additional 24 h. After cooling, the mixture was treated with 1M HCl at 0 °C until pH 6-7 and the yellow precipitate was filtered and washed with diethyl ether and MeOH. The filtered solid was collected and dried under vacuum. The filtrate was condensed and washed with MC and water. The organic layer was condensed again and the precipitate was filtered and washed with MeOH. The afforded yellow powder was collected and dried under vacuum. Yield: 4.00 g, 10.8 mmol, 48%.

^1H NMR (400 MHz, DMSO- d_6 , δ): 8.29–8.21 (m), 8.10–8.07 (m), 7.72 (s), 7.69 (t), 7.61–7.53 (m), 7.19 (s), 4.97 (s).

Synthesis of 2,6-bis(5-phenyl pyrazolyl)pyridine (3-bpp)

3,3'-(pyridine-2,6-diyl)bis(1-phenylpropane-1,3-dione) (5.01 g, 13.5 mmol) was dissolved in MeOH (200ml) and heated to 50 °C under nitrogen atmosphere. The hydrazine monohydrate (6.74 g, 135 mmol, 6.53 ml) was added to the mixture by syringe for 30 min in dropwise. The mixture was refluxed for overnight. After reaction finished, the resulting solution was cooled to room temperature, obtaining precipitate as a white solid. The afforded white powder was filtered and washed with MeOH (200 ml x 3) and dried under vacuum. Yield: 3.50 g, 9.63 mmol, 71.4 %

^1H NMR (400 MHz, DMSO- d_6 , δ): d 13.61 (br, 2H), 8.04 (t, J = 7.6, 1H), 7.92 (d, J = 8.0, 4H), 7.82 (d, J = 7.6, 2H), 7.52 (s, 2H), 7.46 (t, J = 7.6, 4H), 7.34 (t, J = 7.6, 2H). ^{13}C NMR (100 MHz, DMSO- d_6): d 152.1, 147.5, 143.7, 143.1, 139.4, 133.9, 129.5, 129.2, 128.7, 128.1, 125.6, 118.9, 101.2.

Synthesis of 3-bpp-POP

2,6-bis(5-phenyl pyrazolyl)pyridine (3.05 g, 8.39 mmol) was charged in 500 ml of 3-neck round bottom flask with condenser. After cooled to 0 °C, 200 ml of dichloromethane was added by syringe under nitrogen atmosphere. After stirring for 10 minute, AlCl_3 (19.3 g, 145 mmol) was added to the mixture and stirred at 0 °C for 4 h. The mixture was gradually heated stepwise to 30 °C for 8h, 40 °C for 12 h, 60 °C for 12h, and finally to 80 °C for 24h (dark brown). After the reaction finished, 200 ml of 1M HCl solution was added to quench the mixture at 0 °C and stirred for 2 h. The solid was filtered out and washed thoroughly with excess of water, THF, MeOH, and acetone. The filtered solid was subsequently washed with Soxhlet method with MeOH/THF(1:1 volume ratio) for 24 h. The afforded brown powder was dried under vacuum for overnight. (~ 3.1 g)

Synthesis of Ru/3-bpp-POP

3-bpp-POP (1.21 g), $\text{RuCl}_3 \cdot 3\text{H}_2\text{O}$ (0.097 g), and anhydrous methanol (250 ml) were charged into 500 ml of round bottom flask with condenser and stirred for 30 min under nitrogen atmosphere and refluxed for 24 h. After the reaction finished, the mixture was cooled to room temperature and the black colored powder was filtered and washed with excess of methanol (3 x 100 ml), tetrahydrofuran (3 x 100 ml), acetone (3 x 100 ml), and methylene chloride (3 x 100 ml). The filtered powder was dried under vacuum at 100 °C for overnight. (~ 1.25 g)

Hydrogenation procedure

Hydrogenation was performed using stainless steel batch reactor (150 ml). Ru/3-bpp-POP catalyst and levulinic acid dispersed in desired solvents were charged into the batch reactor. The reactor was closed tightly. After flushed with hydrogen to remove air, the reactor was pressurized with hydrogen to the desired pressure at 25 °C. Then the mixture was heated to desired temperature with stirring rate of 250 rpm for 4h. After the reaction finished, the reactor was cooled to room temperature. The products were analyzed by ^1H NMR measurements using maleic acid as an internal standard. The catalyst was recovered for further characterization by filtration method and dried under vacuum overnight at 80 °C for overnight. In recycle tests, the recovered catalyst was used for successive runs by following the similar procedure. (Table S3)

Acknowledgements

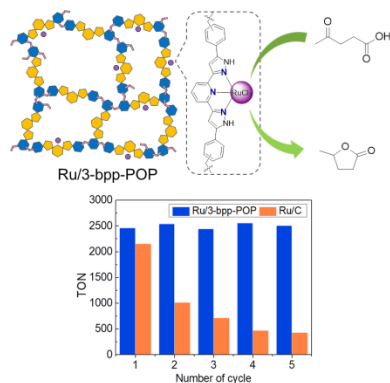
This work was financially supported by the Ministry of Science, ICT & Future Planning (2020M3H7A1098259 and 2020M3H7A1098271) and the Korea Institute of Science and Technology (KIST).

Keywords: heterogeneous catalyst • biomass transformation • porous organic polymer • pincer complexes • levulinic acid hydrogenation

- [1] R. Dawson, A. I. Cooper, D. J. Adams, *Prog. Polym. Sci.* **2012**, *37*, 530-563.
- [2] X. Zou, H. Rena, G. Zhu, *Chem. Commun.*, **2013**, *49*, 3925–3936.
- [3] N. Enjamuri, S. Sarkar, B. M. Reddy, *J. Mondal, Chem. Rec.* **2019**, *19*, 1782-1792.
- [4] K. Dong, Q. Sun, X. Meng, F.-S. Xiao, *Catal. Sci. Technol.* **2017**, *7*, 1028-1039.
- [5] K. Cousins, R. Zhang, *Polymers* **2019**, *11*, 690.
- [6] Y. B. Zhou, Z. P. Zhan, *Chem. Asian J.* **2018**, *13*, 9-19.

- [7] X. Li, X. Yang, Y. Huang, T. Zhang, B. Liu, *Adv. Mater.* **2019**, 31, 1902031.
- [8] J. Su, J.-S. Chen, *Microporous Mesoporous Mat.* **2017**, 237, 246-259.
- [9] F. M. Wigger, Y. Mohr, E. A. Quadrelli, J. Canivet, *ChemCatChem* **2020**, 12, 1270-1275.
- [10] M. Tsyurupa, V. Davankov, *React. Funct. Polym.* **2002**, 53, 193-203.
- [11] J.-Y. Lee, C. D. Wood, D. Bradshaw, M. J. Rosseinsky, A. I. Cooper, *Chem. Commun.* **2006**, 2670-2672.
- [12] S. Xu, Y. Luo, B. Tan, *Macromol. Rapid Commun.* **2013**, 34, 471-484.
- [13] J. Huang, S. R. Turner, *Polym. Rev.* **2018**, 58, 1-41.
- [14] L. Tan, B. Tan, *Chem. Soc. Rev.* **2017**, 46, 3322-3356.
- [15] X. Tang, X. Zeng, Z. Li, L. Hu, Y. Sun, S. Liu, T. Lei, L. Lin, *Renew. Sust. Energ. Rev.* **2014**, 40, 608-620.
- [16] A. D. Patel, J. C. Serrano-Ruiz, J. A. Dumesic, R. P. Anex, *Chem. Eng. J.* **2010**, 160, 311-321.
- [17] J. J. Bozell, G. R. Petersen, *Green Chem.* **2010**, 12, 539-554.
- [18] D. M. Alonso, S. G. Wettstein, J. A. Dumesic, *Green Chem.* **2013**, 15, 584-595.
- [19] Y. Gu, F. Jérôme, *Chem. Soc. Rev.* **2013**, 42, 9550-9570.
- [20] J. Zhang, S. Wu, B. Li, H. Zhang, *ChemCatChem* **2012**, 4, 1230-1237.
- [21] W. R. Wright, R. Palkovits, *ChemSusChem* **2012**, 5, 1657-1667.
- [22] U. Omoruyi, S. Page, J. Hallett, P. W. Miller, *ChemSusChem* **2016**, 9, 2037-2047.
- [23] S. Dutta, K. Iris, D. C. Tsang, Y. H. Ng, Y. S. Ok, J. Sherwood, J. H. Clark, *Chem. Eng. J.* **2019**, 372, 992-1006.
- [24] A. Seretis, P. Diamantopoulou, I. Thanou, P. Tzevelekidis, C. Fakas, P. Lilas, G. Papadogianakis, *Front. Chem.* **2020**, 8, 221.
- [25] F. Liguori, C. Moreno-Marrodan, P. Barbaro, *ACS Catal.* **2015**, 5, 1882.
- [26] C. A. M. R. van Slagmaat, M. A. F. Delgove, J. Stouten, L. Morick, Y. van der Meer, K. V. Bernaerts and S. M. A. De Wildeman, *Green Chem.*, **2020**, 22, 2443-2458.
- [27] J. Tan, J. Cui, T. Deng, X. Cui, G. Ding, Y. Zhu, Y. Li, *ChemCatChem* **2015**, 7, 508-512.
- [28] J. Molletti, M. S. Tiwari, G. D. Yadav, *Chem. Eng. J.* **2018**, 334, 2488-2499.
- [29] C. Xiao, T.-W. Goh, Z. Qi, S. Goes, K. Brashler, C. Perez, W. Huang, *ACS Catal.* **2016**, 6, 593-599.
- [30] M. G. Al-Shaal, W. R. Wright, R. Palkovits, *Green Chem.* **2012**, 14, 1260-1263.
- [31] A. Primo, P. Concepción, A. Corma, *Chem. Commun.* **2011**, 47, 3613-3615.
- [32] X. Gao, S. Zhu, M. Dong, J. Wang, W. Fan, *Appl. Catal. B: Environ.* **2019**, 259, 118076.
- [33] N. M. Patil, B. M. Bhanage, *ChemCatChem* **2016**, 8, 3458-3462.
- [34] C. Ortiz-Cervantes, J. J. Garcia, *Inorg. Chim. Acta* **2013**, 397, 124-128.
- [35] B. Y. Tay, C. Wang, P. H. Phua, L. P. Stubbs, H. V. Huynh, *Dalton Trans.* **2016**, 45, 3558-3563.
- [36] M. Chen, Q. Dong, W. Ni, X. Zhao, Q. Gu, G. Tang, D. Li, W. Ma, Z. Hou, *ChemistrySelect* **2017**, 2, 10537-10545.
- [37] A. Piskun, J. Ftouni, Z. Tang, B. Weckhuysen, P. Bruijninx, H. J. Heeres, *Appl. Catal. A: Gen.* **2018**, 549, 197-206.
- [38] L. Wu, J. Song, B. Zhou, T. Wu, T. Jiang, B. Han, *Chem. Asian J.* **2016**, 11, 2792-2796.
- [39] Z. Meng, Y. Liu, G. Yang, Y. Cao, H. Wang, F. Peng, P. Liu, H. Yu, *ACS Sustain. Chem. Eng.* **2019**, 7, 16501-16510.
- [40] X. Liu, G. Lan, Y. Boyjoo, L. Qian, S. Gu, C. A. H. Price, L. Wang, Y. Li, J. Liu, *Chem. Eng. J.* **2019**, 374, 895-903.
- [41] Z. Wei, X. Li, J. Deng, J. Wang, H. Li, Y. Wang, *Mol. Catal.* **2018**, 448, 100-107.
- [42] J. Ftouni, A. Muñoz-Murillo, A. Goryachev, J. P. Hofmann, E. J. Hensen, L. Lu, C. J. Kiely, P. C. Bruijninx, B. M. Weckhuysen, *ACS Catal.* **2016**, 6, 5462-5472.
- [43] S. Li, Y. Wang, Y. Yang, B. Chen, J. Tai, H. Liu, B. Han, *Green Chem.* **2019**, 21, 770-774.
- [44] J. Pan, Q. Xu, L. Fang, G. Tu, Y. Fu, G. Chen, F. Zhang, W. Zhu, *Catal. Commun.* **2019**, 128, 105710.
- [45] J. Tan, J. Cui, G. Ding, T. Deng, Y. Zhu, Y.-w. Li, *Catal. Sci. Technol.* **2016**, 6, 1469-1475.
- [46] Q. Wang, X. Ling, T. Ye, Y. Zhou, J. Wang, *J. Mater. Chem. A* **2019**, 7, 19140-19151.
- [47] Y. Shen, Q. Zheng, H. Zhu, T. Tu, *Adv. Mater.* **2020**, 32, 1905950.
- [48] Y. Nakahara, T. Toda, A. Matsunami, Y. Kayaki, S. Kuwata, *Chem. Asian J.* **2018**, 13, 73-80.
- [49] Q. Yang, L. Wang, L. Lei, X.-L. Zheng, H.-y. Fu, M.-I. Yuan, H. Chen, R.-X. Li, *Catal. Commun.* **2012**, 29, 194-197.
- [50] K. Umehara, S. Kuwata, T. Ikariya, *J. Am. Chem. Soc.* **2013**, 135, 6754-6757.
- [51] M. A. Halcrow, *Coord. Chem. Rev.* **2005**, 249, 2880-2908.
- [52] E. D. Doidge, J. W. Roebuck, M. R. Healy, P. A. Tasker, *Coord. Chem. Rev.* **2015**, 288, 98-117.
- [53] A. Yoshinari, A. Tazawa, S. Kuwata, T. Ikariya, *Chem. Asian J.* **2012**, 7, 1417-1425.
- [54] Y.-Y. Fang, W.-J. Gong, X.-J. Shang, H.-X. Li, J. Gao, J.-P. Lang, *Dalton Trans.* **2014**, 43, 8282-8289.
- [55] T. D. Roberts, M. A. Halcrow, *Polyhedron* **2016**, 103, 79-86.
- [56] S. Gunnaz, N. Özdemir, S. Dayan, O. Dayan, B. Cetinkaya, *Organometallics* **2011**, 30, 4165-4173.
- [57] L. Wang, Q. Yang, H. Chen, R.-X. Li, *Inorg. Chem. Commun.* **2011**, 14, 1884-1888.
- [58] Y. Zhou, W. Chen, D. Wang, *Dalton Trans.* **2008**, 1444-1453.
- [59] K. S. Sing, *Pure Appl. Chem.* **1985**, 57, 603-619.
- [60] S. P. Brown, *Solid State Nucl. Magn. Reson.* **2012**, 41, 1-27.
- [61] P. Hodgkinson, *Annu. Rep. NMR Spectro.* **2011**, 72, 185-223.
- [62] S. Hou, S. Wang, X. Long, B. Tan, *RSC Adv.* **2018**, 8, 10347-10354.
- [63] G. H. Gunasekar, S. Yoon, *J. Mater. Chem. A* **2019**, 7, 14019-14026.
- [64] P. Leinweber, J. Kruse, F. L. Walley, A. Gillespie, K.-U. Eckhardt, R. I. Blyth, T. Regier, *J. Synchrotr. Radiat.* **2007**, 14, 500-511.
- [65] K. S. Lakhi, D.-H. Park, G. Singh, S. N. Talapaneni, U. Ravon, K. Al-Bahily, A. Vinu, *J. Mater. Chem. A* **2017**, 5, 16220-16230.
- [66] D. J. Morgan, *Surf. Interface Anal.* **2015**, 47, 1072-1079.
- [67] P. J. Dyson, P. G. Jessop, *Catal. Sci. Technol.* **2016**, 6, 3302-3316.
- [68] Y. Yi, H. Liu, L.-P. Xiao, B. Wang, G. Song, *ChemSusChem* **2018**, 11, 1474-1478.
- [69] B. P. Pinto, A. L. L. Fortuna, C. P. Cardoso, C. J. A. Mota, *Catal. Lett.* **2017**, 147, 751-757.
- [70] J. Moritani, Y. Kayaki, T. Ikariya, *RSC Adv.* **2014**, 4, 61001-61004.
- [71] C. Moustani, E. Anagnostopoulou, K. Krommyda, C. Panopoulou, K. G. Koukoulakis, E. B. Bakeas, G. Papadogianakis, *Appl. Catal. B: Environ.* **2018**, 238, 82-92.
- [72] J. F. Sonnenberg, N. Coombs, P. A. Dube, R. H. Morris, *J. Am. Chem. Soc.* **2012**, 134, 5893-5899.
- [73] E. Sondaz, A. Gourdon, J.-P. Launay, J. Bonvoisin, *Inorg. Chim. Acta* **2001**, 316, 79-88.
- [74] P. Ghosh, P. Mondal, R. Ray, A. Das, S. Bag, S. M. Mobin, G. K. Lahiri, *Inorg. Chem.* **2014**, 53, 6094-6106.
- [75] M. Ramesh, M. Kalidass, M. Jaccob, D. Kaleeswaran, G. Venkatachalam, *J. Organomet. Chem.* **2017**, 830, 33-41.
- [76] R. H. Morris, *Inorg. Chem.* **2018**, 57, 13809-13821.
- [77] G. H. Gunasekar, K.-D. Jung, S. Yoon, *Inorg. Chem.* **2019**, 58, 3717-3723.

Entry for the Table of Contents



A ruthenium molecular catalyst supported on NNN pincer ligand functionalized porous organic polymer (Ru/3-bpp-POP) is fabricated showing a promise as high-performance and -stability catalyst for levulinic acid hydrogenation to γ -valerolactone.